Check for updates

Two-dimensional multiferroics

Yunye Gao, [a] Mingyuan Gao [a,b] and Yuerui Lu [*a]

Due to unprecedented application prospects such as high-density and low-power multistate storage, spintronics and nanoelectronics, two-dimensional (2D) multiferroics, coupled with at least two ferroic orders, have gotten a lot of interest in recent years. Multiple functions can be achieved in 2D multiferroics *via* coupling phenomena such as magnetoelectricity, piezoelectricity, and magnetoelasticity, which offers technical support for the creation of multifunctional devices. The research progress of 2D ferromagnetic–ferroelectric multiferroic materials, ferroelectric–ferroelastic multiferroic materials, and ferromagnetic–ferroelastic materials in recent years is reviewed in this paper. The categorization of 2D multiferroics is explored in terms of the multiple sources of ferroelectricity. The top-down approaches and the bottom-up methods used to fabricate 2D multiferroics materials are introduced. Finally, the authors outline potential research prospects and application scenarios for 2D multiferroic materials.

1. Introduction

Multiferroic materials, which are multifunctional materials with numerous main ferroic orders in a single phase, are fundamentally and technologically essential for a variety of applications, such as nonvolatile memory,[1] sensors,[2] energy harvesting,[3] and actuators,[4] among others.[5–9] Ferroelectricity (FE), which breaks space-inversion symmetry, ferromagnetism (FM), which breaks time-reversal symmetry and ferroelasticity (FA), which breaks neither space-inversion symmetry nor time-reversal symmetry, are the well-known primary ferroic orders, which can be switched by their conjugate electric (E), magnetic (H), and stress (σ) fields, respectively. Ferrotoroidicity (FT), which breaks both the space-inversion and the time-reversal symmetry, should be switchable by crossed magnetic and electric fields, in addition to these three typical ferroic orders
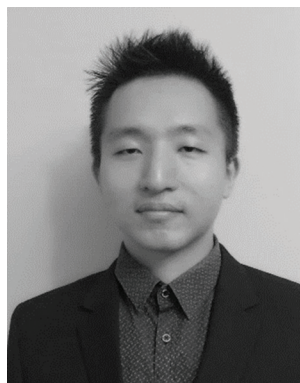
[a]School of Engineering, College of Engineering and Computer Science, the Australian National University, Canberra, Australian Capital Territory 2601, Australia.
E-mail: yuerui.lu@anu.edu.au
[b]College of Engineering and Technology, Southwest University, Chongqing 400716, China

Yunye Gao is a PhD candidate in the School of Engineering, College of Engineering and Computer Science at the Australian National University. She earned her BE degree from Zhejiang Normal University, China, in 2020. Her research interests include two-dimensional multiferroics and piezoelectric actuators.

Yunye Gao

Mingyuan Gao is an Associate Professor in the College of Engineering and Technology at Southwest University, China, and a Postdoctoral Researcher in the College of Engineering and Computer Science at the Australian National University. He earned his BE and ME degrees from Huazhong University of Science and Technology, China, in 2008 and 2010, respectively, and his PhD degree from Southwest Jiaotong University in 2018. He was a Senior Mechanical Engineer in Siemens AG from 2011 to 2018. His research interests include flexible electronics, energy harvesting, self-powered monitoring, and nonlinear dynamics. He won the 2010 GE Foundation TECH Award-First Place Award.
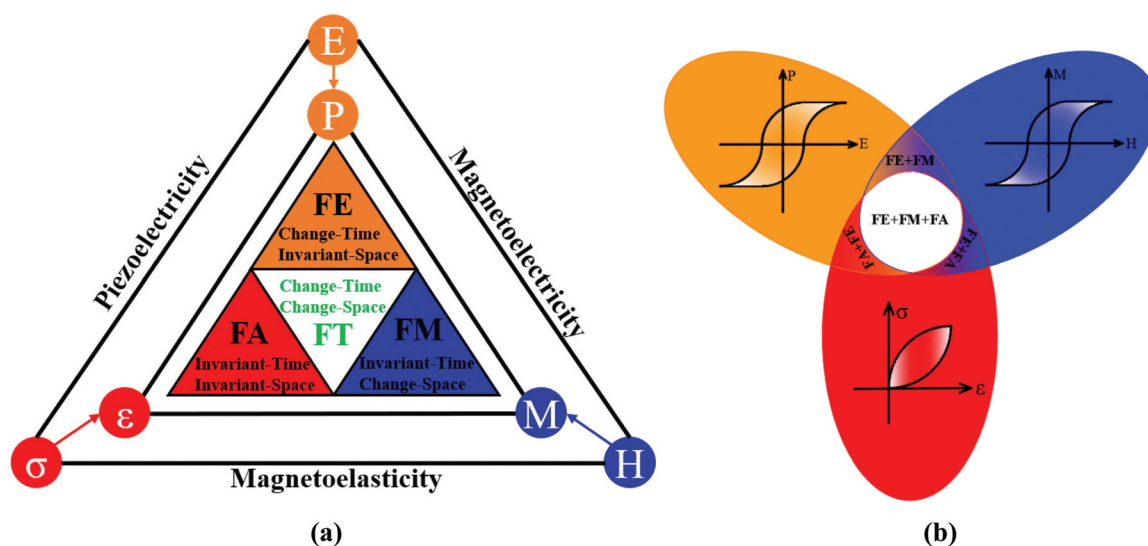
Mingyuan Gao

Fig. 1 Different ferroic orders corresponding to the different time and space reversal symmetry and mutual cross-coupling between orders *via* magnetoelectric, piezoelectric, or magnetoelastic interactions. (a) FE breaking space-inversion symmetry; FM breaking time-reversal symmetry; FA breaking neither space-inversion symmetry nor time-reversal symmetry and FT breaking both space-inversion symmetry and time-reversal symmetry. (b) Mutual cross-coupling between ferroic orders. Redrawn based on ref. 25.

(Fig. 1(a)). Multiferroics exhibit unique properties due to mutual cross-coupling between ferroic orders *via* magnetoelectric, piezoelectric, or magnetoelastic interactions. In a ferromagnetic–ferroelectric multiferroic, an electric field can tune the magnetization and a magnetic field can tune the electric polarization; in a ferroelectric–ferroelastic multiferroic, stress fields can tune the electric polarization, and an electric field can tune the magnetization (Fig. 1(b)) This allows the design and assembly of numerous multipurpose devices to fulfil the conceivable and promising demands of individuals and indus-

Yuerui Lu is an Associate Professor in the College of Engineering and Computer Science at the Australian National University. He received his PhD degree from Cornell University, School of Electrical and Computer Engineering, in 2012. He holds a BS degree from the Department of Applied Physics at the University of Science and Technology of China. His research interests include MEMS/NEMS sensors

Yuerui Lu

and actuators, nano-manufacturing technologies, renewable energy harvesting, biomedical novel devices, nanomaterials, and nanoelectronics. He was the recipient of several awards, including the competitive ACT Young Tall Poppy of 2016, and the Media and Outreach Award from Australian National University in 2015.

tries. The ferromagnetic–ferroelectric multiferroic material, for example, allows for efficient writing and reading for high-density data storage while consuming minimal energy.

However, most materials, particularly multiferroic materials, face significant technological challenges in terms of downsizing and integration, prompting scientists to seek out low-dimensional multiferroic materials of atomic thickness. Low-dimensional materials, as opposed to three-dimensional (3D) multiferroic materials, generally have smooth surfaces and high dielectric constants, making nanoscale devices possible. Since graphene was physically exfoliated from graphite in 2004,[10] a wide range of 2D materials has been discovered and studied, including monochalcogenides,[11,12] transition-metal phosphorus chalcogenides,[13] phosphorene,[5,14,15] molybdenum disulfide,[16,17] transition-metal dichalcogenides,[18–23] transition/rare-earth metal halides[24] and so on.

In this paper, we discuss current research advances in 2D multiferroic materials over the last decade. We will look at the theoretical calculations and experimental discoveries of 2D multiferroics, as well as the categorization and preparation of 2D multiferroic materials, and future research possibilities for these materials.

2. Experimental and theoretical progress on 2D multiferroic materials

The past decade has witnessed remarkable progress in understanding of multiferroicity in 2D materials largely due to theoretical investigations based on DFT (first-principles density functional theory) and experimental observations.

2.1 Research progress of 2D ferromagnetic–ferroelectric multiferroics

Due to the coexistence of the characteristics of the two-parent compounds and additional functions from the interaction between magnetic polarization and electrical polarization, multiferroic materials that are both ferroelectric and ferromagnetic may be more prevalent and diverse than traditional multiferroics, allowing for energy storage and efficient writing by an electric field. They are, however, uncommon for the following reasons: (1) ferroelectrics are insulators by definition, whereas itinerant ferromagnets require conduction electrons; (2) magnetism is typically caused by ordered spins of electrons in d/f orbitals partially filled by transition metals, whereas FE is frequently caused by residual polarization caused by stable off-centered ions with empty d/f orbitals. Ascher et al. reported the magnetoelectric coupling in bulk $Ni_3B_7O_{13}I$ for the first time in 1966.[26] Following that, 2D multiferroic materials with magnetoelectric coupling effects, such as CrI_3 with I vacancy,[27] (TMPCs)-$CuMP_2X_6$ (M = Cr, V; X = S, Se),[28] 2D ferromagnets MXene, VS_2 and MoN_2,[11] monolayer carbides and carbon nitrides (MXenes) $Hf_2VC_2F_2$ monolayer,[29] $VOCl_2$ monolayer[30] and other thin-film growth approaches have also been investigated. It is worth noting that VOI_2 monolayer[31,32] is either a ferroelectric magnet with spiral-spin configuration or a ferromagnetic metal, instead of a ferromagnetic–ferroelectric multiferroic, due to the presence of the heavy element iodine with a strong spin–orbit coupling, which produces an effective Dzyaloshinskii–Moriya interaction in a polar structure. Tu et al. published the first 2D organic multiferroics with coexisting ferromagnetic and ferroelectric characteristics in 2017, based on theoretical observation of the C_6N_8H organic network (Fig. 2(a)), allowing for the construction of a 2D multifunctional integrated circuit. Using DFT, monolayer transition metal phosphorus chalcogenides were confirmed to be 2D multiferroic semiconductors with strongly coupled ferroelectric and ferromagnetic orders in 2018, in which FM is caused by indirect exchange interaction between Cr/V atoms and FE is caused by copper atoms spontaneously moving away from the central atomic plane (Fig. 2(c)). These kinds of materials pave the way for 2D multiferroic switches and memories. Gao et al. in 2020 reported magnetoelectric coupling produced by Fe in a 2D $BaTiO_3(001)$ ultrathin film (see Fig. 2(b)), in which the Fe impurity enhances the overall magnetic moment but inhibits spontaneous polarization. This research suggests that by carefully replacing Ti atoms with Fe atoms, 2D $BaTiO_3$ may be made into a multiferroic material. Zhong et al. explored a 2D thin-layer $CuCrX_2$ (X = S or Se) multiferroic with the desired coexistence of FM and FE and high magnetoelectric coupling (Fig. 2(d)). Furthermore, the interlayer coupling parameter gradient between neighboring layers resulted in a variety of magnetoelectric layers of various thicknesses. It not only cleared the path for room-temperature ferromagnetic–ferroelectric multiferroicity with significant magnetoelectric coupling, but it also has the potential to spur additional study into multiferroicity in 2D systems.

2.2 Research progress of ferroelectric–ferroelastic multiferroics

Ferroelectric–ferroelastic multiferroics are a kind of 2D multiferroic material with strong spontaneous ferroelectric polarization and spontaneous ferroelastic lattice strain, which is thermodynamically stable at room temperature and higher and can be effectively controlled by elastic strain engineering. In 2017, Wang and Qian predicted that 2D monolayer group IV monochalcogenides MX (M = Ge, Sn and X = S, Se), are a class of 2D ferroelectric–ferroelastic multiferroics (Fig. 3(a)), which has the potential to become multifunctional equipment, including 2D ferroelastic memory, 2D ferroelectric memory, 2D ferroelectric excitonic photovoltaics, and 2D ferroelectric–ferroelastic nonvolatile photonic memory. In the same year, a group of researchers predicted the giant second harmonic (SHG)[37,38] in the newly revealed 2D ferroelectric–ferroelastic multiferroic materials (group IV monochalcogenides) (Fig. 3(b)), which paved a range of new ways for multiferroic materials, nonlinear optoelectronics and 2D ferroelectrics, among other things. For example, by utilizing noncontact non-invasive optical SHG methods, it can achieve ultrafast optical characterization of local electronic and atomistic structures and active mechanical/optical/electrical switching of ferroic orders in 2D multiferroics. Wu and Zeng revealed, in 2017, that Bi_2O_2Se, Bi_2O_2S and Bi_2O_2Te (Fig. 3(c)), are multiferroics possessing FE and FA, which makes it possible to integrate the room temperature functional nonvolatile memories (NVM) into future nanocircuits. Besides, the good matching of the lattice constants of the bismuth oxychalcogenide makes the heterostructure devices have no lattice mismatch problems, to be tailored to the application. In 2017, a multiferroic material with linked FA and FE was anticipated for the Boron pentaphosphide (BP_5) monolayer (Fig. 3(d)). The expected reversible strain is the highest among all ferroelastic materials (41.41%). In BP_5, the spontaneous in-plane polarization is due to the difference in electronegativity between the phosphorus and boron atoms and the non-centrosymmetric structure. It has been proposed as a possible nanomaterial for the construction of optoelectronic or electromechanical devices, such as nonvolatile memory with easy read/write capabilities. Gao et al. revealed in 2019 that silver/copper mono-halides had linked FE and FA, as well as modest switching barriers (Fig. 3(e)). Using basic principles, Zhang et al. discovered in 2021 that bilayer ZrI_2 (Fig. 3(f)) not only retains the in-plane and out-of-plane polarization caused by the redistribution of charges between layers but also has FA due to its crystal symmetry. It described a new design concept that achieves ferroelastic FE by using van der Waals interaction as a disturbance in a double-layer lattice. This approach provides a new way for 2D ferroelastic FE to be realized and developed.

2.3 Research progress of ferromagnetic–ferroelastic multiferroics

Both ferromagnetic and ferroelastic orders could be found in ferromagnetic–ferroelectric multiferroics. Seixas et al. revealed
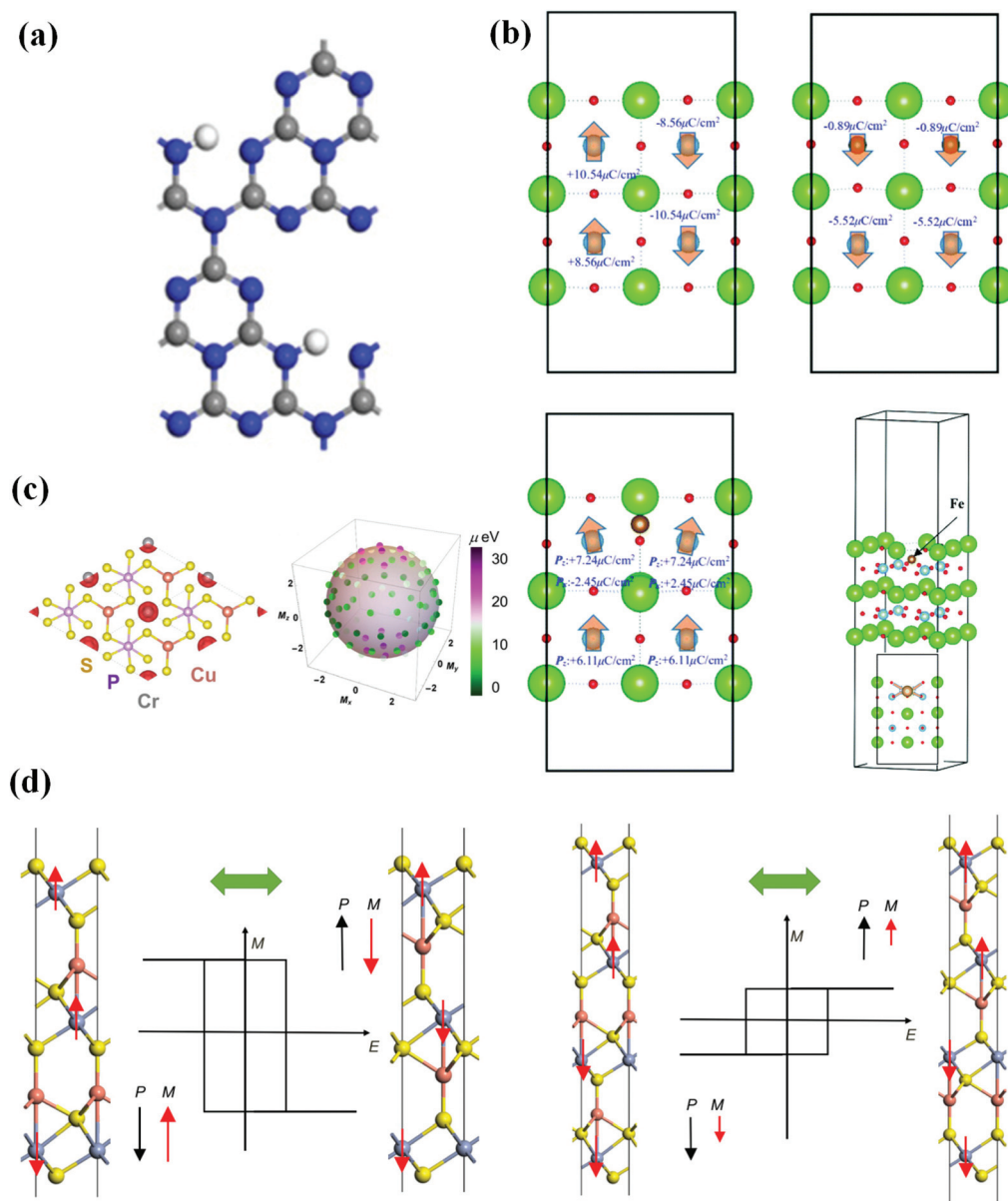
(a)

(b)

(c)

(d)

Fig. 2 Several 2D ferromagnetic–ferroelectric multiferroic materials in recent years. (a) Optimized structure of C_6N_8H. Reproduced with permission.[33] 2017, American Chemical Society. (b) Ferroelectric characteristics of 2D $BaTiO_3$ ultrathin film without and with Fe. Reproduced with permission.[34] Copyright 2020, The Royal Society of Chemistry. (c) Ferroelectric and magnetic characteristics of monolayer $CuCrP_2S_6$. Reproduced with permission.[35] Copyright 2018, AIP Publishing. (d) Geometric structures and multiferroic conversion of $Cu_2(CrS_2)_3$ (left) and $Cu_3(CrS_2)_4$ (right) thin films. Reproduced with permission.[36] Copyright 2020, China Science Publishing & Media.

in 2016 that depending on the hole density, the α-SnO monolayer (Fig. 4(a)) can be ferromagnetic, ferroelastic, or even multiferroic. In other words, a new class of multiferroic 2D systems is discovered in a range of hole densities where the material exhibits both FM and FA. These materials open up new avenues for developing flexible memory and integrating them with other flexible electronics. In 2020, Xu *et al.* suggested a new 2D multiferroic material (single-layer AgF_2) as an antiferromagnetic ferroelastic semiconductor with high spin polarization (Fig. 4(b)). The presence of antiferromagneticity and FA in the AgF_2 monolayer is important for the study of

2D multiferroics and makes it a viable platform for future multifunctional device applications. In 2020, Xu *et al.* reported that magnetic easy axes in 2D ferromagnets: CrSX (X = Br, I, Cl) monolayers could be switched by ferroelastic strain (Fig. 4(c)), showing that these monolayers are 2D multiferroic materials. By integrating ferroelastic phase transition, these discoveries give a potential framework for controlling spintronic characteristics. Pang *et al.* proposed in 2021 that 2D tetragonal structures XOBr (X = Ru, Tc) (Fig. 4(d)) are multiferroic semiconductors with significant electrical anisotropy, FA, and coexisting ferromagnetic characteristics. The ferroelastic switch may be used to modify
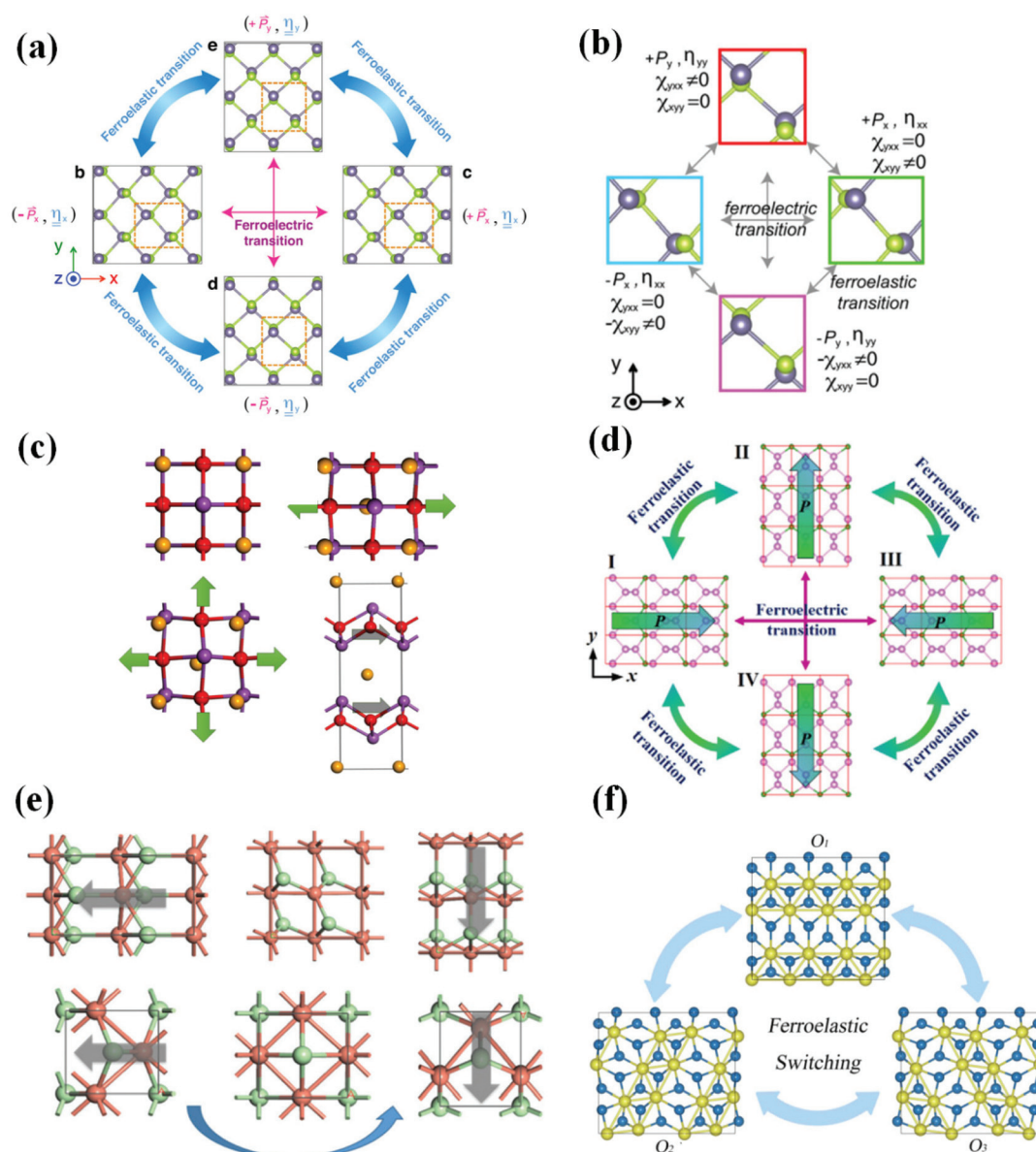
Fig. 3 Several 2D ferroelectric–ferroelastic multiferroic materials in recent years. (a) Ferroelastic and ferroelectric transition of monolayer group IV monochalcogenides. Reproduced with permission.[39] Copyright 2017, IOP Publishing. (b) Ferroelastic and ferroelectric transition of monolayer GeSe. Reproduced with permission.[40] Copyright 2017, American Chemical Society. (c) Geometry of Bi_2O_2Se under uniaxial and biaxial strain. Reproduced with permission.[41] Copyright 2017, American Chemical Society. (d) Ferroelastic and ferroelectric transition of BP_5. Reproduced with permission.[14] Copyright 2017, IOP Publishing. (e) Ferroelastic switching of 2D polymorphs of CuCl. Reproduced with permission.[42] Copyright 2019, The Royal Society of Chemistry. (f) Ferroelastic switching of monolayer ZrI_2. Reproduced with permission.[43] Copyright 2021, American Physical Society.

the direction of anisotropic electron behaviour by applying external stress. The findings support the creation of electrical and memory devices that can be controlled.

In general, disclosed 2D multiferroics, whether ferromagnetic–ferroelectric, ferroelectric–ferroelastic, or ferromagnetic–ferroelastic, are extremely rare; the majority of them were postulated based on theoretical simulations, with little practical advances as far. More significantly, the vast majority of theoretically postulated multiferroic characteristics are type I; few materials have strong ferroic coupling. 2D multiferroic materials have yet to be used in practical applications. This intriguing but mostly unexplored field of study offers enormous possibilities for the academic community.

3. Classification of 2D multiferroics

3.1 Classification of multiferroics

There are two classification criteria for multiferroic materials: one is based on the coupling effect between the ferroic orders,
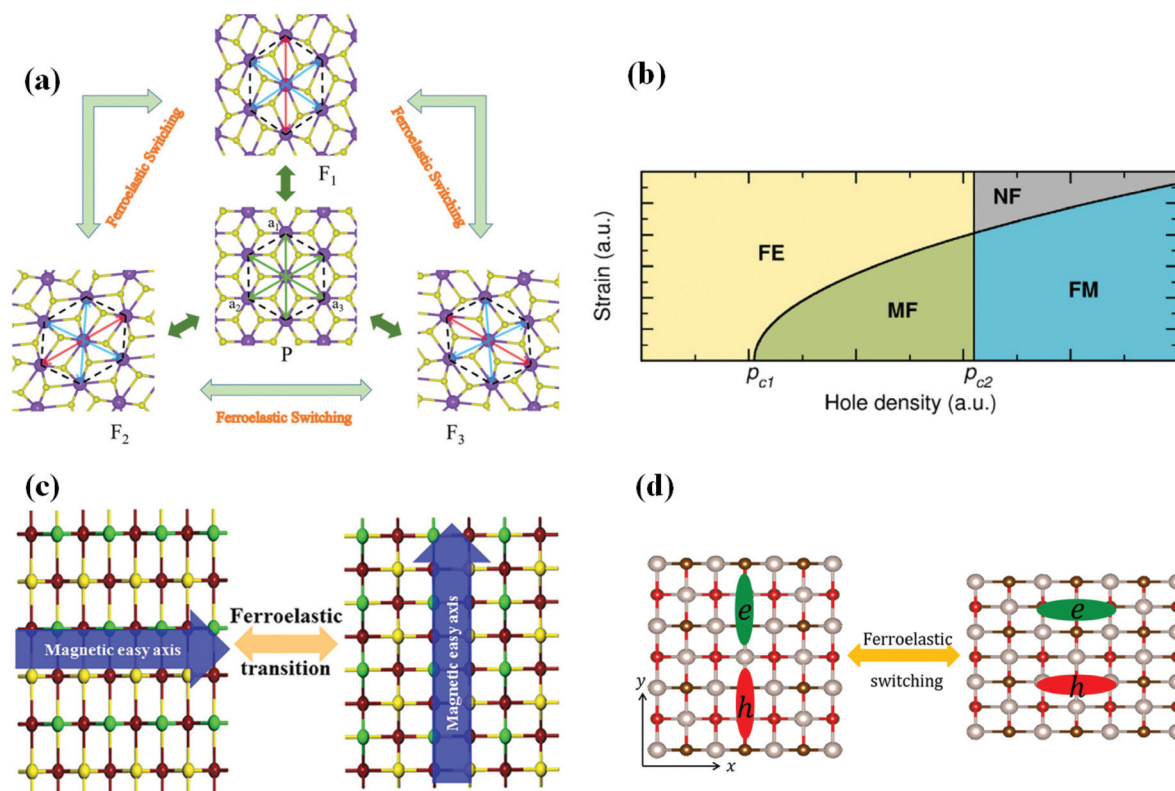
Fig. 4 Several 2D ferromagnetic–ferroelastic multiferroic materials in recent years. (a) Ferroelastic switching of the monolayer AgF_2. Reproduced with permission.[44] Copyright 2020, The Royal Society of Chemistry. (b) Schematic diagram of the generalized Landau model in a multiferroic (FM and FA) α-SnO monolayer. Reproduced with permission.[45] Copyright 2016, American Physical Society. (c) The ferroelastic transition of the CrSI monolayer. Reproduced with permission.[46] Copyright 2020, AIP Publishing. (d) Ferroelastic switching of TcOBr. Reproduced with permission.[47] Copyright 2020, Elsevier.

namely, ferroelectric–ferromagnetic, ferromagnetic–ferroelastic, and ferroelectric–ferroelastic multiferroics corresponding to magnetoelectric, piezoelectric and magnetoelastic effect, respectively. The other is proposed by Khomskii in 2009 to divide multiferroics into two categories, *i.e.* type-I and type-II multiferroic materials[48,49] (Fig. 5(a)). With regard to type-I multiferroics, the origins of FE and FM are different and the coupling between FE and magnetism is usually weak. According to current reports, type-I multiferroics are more common with large polarization and high transition temperatures. In contrast, type II multiferroic materials, in which FE only appears in a magnetically ordered state that breaks the inversion symmetry, are more attractive in applications due to the strong coupling between FE and magnetism.

3.1.1 Type-I multiferroics. Based on the microscopic mechanism of FE in 2D type-I multiferroics, it can be divided into three subgroups: (i) lone-pair multiferroics; (ii) charge-ordered multiferroics; (iii) geometrically frustrated multiferroics.

Typical multiferroics, $BiFeO_3$,[50] $BiMnO_3$[51] and $PbVO_3$,[52] belong to the lone-pair category, where cations owing highly polarizable $6s^2$ lone-pair electrons (Bi^{3+} and Pb^{2+}) play a major role in the origin of FE and have high polarizability.

Charge-ordered multiferroics are often observed in transition metal compounds with ions that formally have a mixed valence. Typically, site-centered charge order and bond-centered charge order are two general types, where mirror planes of the charge order structure can be marked at ions or bond centers. In order to realize FE in charge-ordered multiferroics, it is necessary to combine these two charge orders, namely, the existence of inequivalent sites and bonds in the system at the same time. Some systems like an organic ferroelectric $(TMTTF)_2X$[53] or multiferroic $LuFe_2O_4$[54] are inequivalent due to their different crystallographic structures, and a spontaneous charge ordering drives the inequivalence of the sites. *Vice versa*, in some materials containing ions with different valences, $TbMn_2O_5$[55] and multiferroic Ca_3CoMnO_6,[56] after a structural dimerization transition can be induced to be ferroelectric.

The last mechanism leading to type-I multiferroicity may be frustrated geometry in multiferroics, as the geometrical effect of increasing the packing density can lead to permanent dipoles and FE. Hexagonal $YMnO_3$[57] and non-magnetic K_2SeO_4[58] belongs to this class. For example, in $YMnO_3$, magnetic Mn^{3+} does not affect FE, but the tilting of the practically rigid MnO_5 block is the main cause of FE. As a consequence,
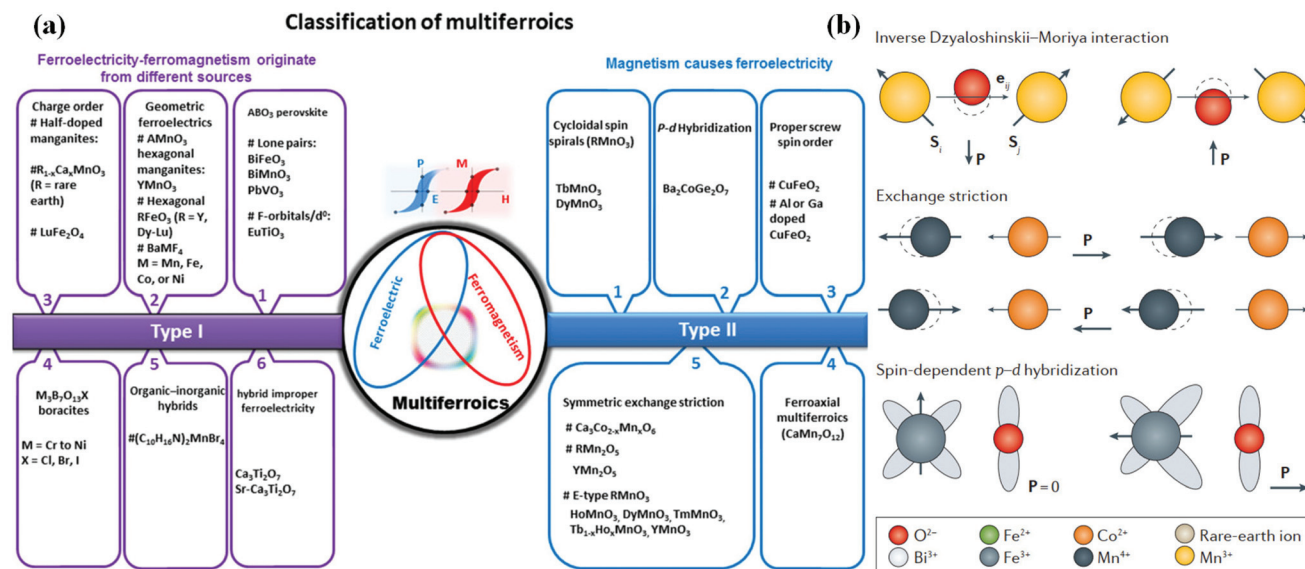
Fig. 5 Microscopic mechanisms of FE in type-II 2D multiferroics. (a) The classification of the multiferroic materials into two types with subclass groups. Reproduced with permission.[60] Copyright 2021, Springer Nature. (b) Three major microscopic mechanisms of FE in type-II multiferroic materials. Reproduced with permission.[61] Copyright 2014, IOP Publishing.

the oxygen ions are closer to the small Y ions due to the occurrence of this tilt, which is only to provide a closer packing.

3.1.2 Type-II multiferroics. Another way of achieving multiferroicity and enhancing magnetoelectric coupling is to produce phase changes through magnetic phase transitions. Theoretically, the structural phase change of the crystal is essential for the generation of FE, but it is not a condition for magnetic order. Magneto-ferroelectricity was first proposed by Khomskii,[48,59] who proposed the term 'type-II multiferroics'. This novel ferroelectric formation mechanism is named the spin magnetic order mechanism, as shown in Fig. 5(b). According to related mechanisms, they can be further subdivided into (1) spin current model; (2) exchange striction; (3) spin-dependent p–d hybridization.

(1) The spin–current mechanism can also be called the anti-DM interaction mechanism. First, the DM interaction is introduced: the super-exchange interaction is modified by the theory of relativity after the spin–orbit coupling. The vector of DM can be regarded as proportional to the displacement of related atoms. When the perovskite structure is distorted, the DM interaction leads to the appearance of a non-collinear spin structure. For this structure, the anti-DM interaction causes the related atoms to move towards moving by Δd in a certain direction, this deviation breaks the symmetry and leads to electric polarization, and the polarization direction has a certain relationship with the spiral axis and the propagation direction of the vector. Such materials include $TbMnO_3$, *etc.*

(2) In the exchange-striction mechanism, the exchange between each adjacent magnetic ion in the magnetic material is affected by the bond length and bond angle. Assuming the existence of frustration in the spin of the magnetic ion, when the spins are parallel, the bond length becomes shorter and

the bond angle becomes smaller, which is beneficial to the reduction of energy, and the opposite is true when the spins are antiparallel. Due to the exchange effect, local electric polarization occurs when the ion position changes and macroscopic electric polarization may appear in special materials. In this mechanism, the direction of ion spin has nothing to do with the direction of electrical polarization. The magnetic field cannot change the direction of electrical polarization, but it can destroy the related sequence and inhibit the generation of electrical polarization. Such materials are: Ca_3CoMnO, R_2CoMnO_6 and so on.

(3) Within spin-dependent p–d hybridization mechanism, the local electric polarization is related to each magnetic ion. The spin–orbit coupling can affect the hybridization between the d orbital and the p orbital, and electric polarization occurs along the direction of the bond. If a space group with relatively low symmetry is used to avoid the cancellation of local electric polarization, the non-centrosymmetric space group will produce polarization. Such materials include Ba_2CoGeO_7, *etc.*

The outstanding advantage of type II multiferroic materials is that the magnetoelectric coupling effect is very strong, because its magnetism and FE are from the same source, and the ferroelectric polarization and magnetic transition occur at the same time. But the shortcomings of this material are also obvious: the FE is relatively weak, the transition temperature is very low, and it does not have the possibility of room-temperature operation. The use of doping or other modified methods to increase the transition temperature and FE is a common research idea for this type of material.

3.2 Classification of 2D multiferroics

2D multiferroic materials can be divided into the intrinsic type and extrinsic type according to the different origins of FE. The

spontaneous ferroelectric polarization in intrinsic 2D multiferroic materials is derived from the structural symmetry of the materials themselves. Extrinsic 2D multiferroics mainly generate ferroelectric properties by selectively exerting external effects.

3.2.1 Intrinsic 2D multiferroics. In recent years, some theoretical work based on first principles has predicted the existence of multiferroics in 2D materials. The following types are the most common, including group IV monochalcogenides, transition metal phosphorus chalcogenides, transition metal thiophosphate, perovskites, transition metal oxyhalide, double transition metal carbides, 2D ferromagnets and bismuth Oxychalcogenides.

Zeng,[12] Wang[39] and Qian[40] all found that the monolayer group IV monochalcogenides MX has a large spontaneous polarization in the plane and spontaneous ferroelastic lattice strains due to their similar structure to black phosphorus through first-principles calculations. Transition-metal-doped group-IV monochalcogenides,[62] monolayer Li-doped GdI_3,[63] γ-GeSe[64] and α-In_2Se_3[65] not only have FE and FA but also have FM due to the doping of transition metal elements. Doping magnetic atom Fe or Mn into 2D ferroelectric crystals (In_2Se_3[66] or SnTe[67]) can also achieve 2D multiferroic materials with magnetoelectric coupling. Transition metal phosphorus chalcogenides (TMPCs)-ABP_2X_6 (A = Cu, Ag, Sc; B = Cr, V; X = S, Se)[13,28,68] has been proved theoretically and experimentally to be a 2D multiferroic material with magnetoelectric coupling effect and its ferroelectric polarization stems from the transition metal elements. Transition metal thiophosphate (TMTP) has also attracted the attention of researchers. The chemical formula of TTMP is $M_x^I M_y^{II} P_2(S/Se)_6$, which is also a type of van der Waals Ears layered materials, some of which can be converted to 2D ferroelectric ferromagnetic materials by constructing van der Waals heterostructures, such as $CuInP_2S_6$/InSe.[69] Perovskites including rare earth manganites ($RMnO_3$) perovskites thin films (R is a rare earth element),[70] $BaTiO_3$ ultrathin film,[34] double-perovskite bilayer with the Fe–Os combination[71] and calcium-based double perovskite double layer,[72,73] have been reported to be 2D multiferroic materials with spontaneous ferroelectric polarization, where the FE is induced by a specific octahedral rotation in a perovskite bilayer. The transition metal oxyhalide $VOCl_2$ monolayer[30] was first proposed in 2018 and has been theoretically proved to have spontaneous FE and multiferroicity. Subsequently, other materials in this family (such as VOF_2;[74] VOF;[75] VOI_2;[31] XOBr (X = Tc, Ru);[47] $FeTe_2O_5Br$[76]) were also confirmed to be intrinsically multiferroic. Besides, metal halides, such as $CrNCl_2$ monolayer,[77] silver and copper monohalides (AgI, CuCl),[42] bilayer VS_2[78] and ZrI_2,[43] monolayer GaTeCl,[79] monolayer AgF_2[44] and vanadium tetrafluoride (VF_4),[80] also belong to this category of multiferroic materials. Double transition metal carbides $Hf_2MC_2T_2$,[29] magnetic transition metal dichalcogenides (H type VS_2, Janus-VSSe, and VSe_2),[81] thin-layer $CuCrX_2$ (X = S or Se),[36] are also been reported to be 2D multiferroic materials with spontaneous ferroelectric polarization.

In 2017, Wu et al.[11] reported the first-principles evidence of 2D vertical FE induced by interlayer translation in some ferro-

magnetic 2D materials such as MXene, VS_2 and MoN_2, which can be even multiferroics with switchable magnetizations upon ferroelectric switching, rendering efficient reading and writing for high-density data storage. In addition, the research group conducted a series of studies on low-dimensional ferroelectric–ferromagnetic coupling and was the first to theoretically predict that C_6N_8H[33] is a 2D organic multiferroic material with ferroelectric–ferromagnetic coupling, giving the 2D organic multiferroic material potential application value in electronic devices. In addition to the 2D ferromagnetic materials with double-layer structure, it is found that the single-layer ferromagnets CrSX (X = Cl, Br, I)[35] also accords with the property of intrinsic multiferroics. In 2017, 2D hyperferroelectric metals CrN and CrB_2[82] was proved to be magnetoelectric multiferroics, where the magnetism can be controlled by the spontaneous out-of-plane electric polarization. Another 2D intrinsic one is bismuth Oxychalcogenides,[41] such as Bi_2O_2S, Bi_2O_2Se and Bi_2O_2Te, possessing intrinsic out-of-plane FE.

In addition to the materials mentioned above, many novel 2D intrinsic multiferroic materials have been proposed. For example, BP_5 monolayer[14] has also been theoretically predicted to be a 2D multiferroic material, where a spontaneous polarization in the plane was produced due to the non-centrosymmetric structure and electronegativity difference between boron and phosphorus atoms. In 2020, $ReWCl_6$ monolayer[83] exhibiting two different low-symmetric phases with opposite in-plane electric polarization and different magnetic order also belongs intrinsic type. Moreover, 2D organometallic frameworks such as $K_3M_2[PcMO_8]$[84] with intrinsic ferro-/ferrimagnetism and vertical FE has been regarded as a versatile platform for designing multifunctional materials with simultaneous ferro-/ferrimagnetism and vertical FE. There are other multiferroic materials whose electric polarization stem from its structure, like NiH_2SeO_4,[85] CrN monolayer,[86] $VOCl_2$,[87] Nb_2ATe_4(A = Si, Ge),[88] α-SnO[45] and FeOOH.[89] Although the multiferroicity of 2D materials is mostly theoretically predicted, the multiferroicity of some materials has also been experimentally verified. In 2017, Zhou et al.[90] gave experimental evidence of the out-of-plane piezoelectric and spontaneously ferroelectric properties of α-In_2Se_3 nanosheets.

3.2.2 Extrinsic 2D multiferroics. Extrinsic 2D multiferroic materials produce spontaneous FE through external effects, including electron or hole doping, defect engineering and surface functionalization.

Electron or hole doping is generally performed to change the electronic structures of materials to modulate specific properties. Doping one electron[91] in the $CrBr_3$ primitive cell has induced the in-plane ferroelectric polarization. Take $(CrBr_3)_2Li$ as an example, the in-plane ferroelectricity is ensured by the combination of charge order and orbital order. When an extra electron is doped in every two Cr–Br_6 octahedra, the asymmetric Jahn–Teller distortions of two neighbouring Cr–Br_6 units are generated, inducing the combination of charge order and orbit order in the material. Hence, the doped-electron-induced charge order and orbit order result in the in-plane fer-

roelectric polarization. This mechanism is not restricted to the above systems but can also be applied to other transition-metal halides and related 2D systems. These findings reveal the existence of multiferroicity in 2D systems and provide a new ideal platform to study 2D multiferroics.

In Defect Engineering, defects can be easily introduced to break the structural symmetry of 2D materials. For example, with the formation of I vacancies in 2D monolayer chromium triiodide (CrI_3), the symmetry of the charge density distributions on top and bottom surfaces is broken, suggesting that there be an out-of-plane polarization in $IV–CrI_3$.[27] Moreover, the ferromagnetic ordering of CrI_3 is not broken by I vacancies, but its ferromagnetism is enhanced. The same case has been found in 2D $BaTiO_3$ ultrathin film with surface Ba vacancy.[92] In this case, the spontaneous polarization parallel is observed, and a magnetic moment in the film stem from the O atoms. The strategy, utilizing surface vacancies to engineer 2D switchable polarization is applicable to many other metal trihalides, such as CrF_3, $CrCl_3$, and YCl_3.

Surface functionalization by atoms or functional groups has been reported to produce spontaneous FE or FM, achieving multiferroicity in 2D materials. In 2017, Wu's research group[93] found through first-principles calculations that the halogen-intercalated phosphorene bilayer not only produces vertical plane polarization but also has "movable" magnetism. Similarly, in the Li-decorated α-Fe_2O_3 monolayer,[94] FE and FM stem from the same origin, namely Fe d-orbital splitting induced by the Jahn–Teller distortion and associated crystal field changes. For CH_2OCH_3-functionalized germanene,[95] the electric polarization is caused by field-induced ligand molecule rotation and the FM stem from a spin-polarized charge distribution on unpassivated Ge sites. Besides, immersing carbon nitrides in the solution of metal halides[96] also makes their cavities can be spontaneously FE, FM or multiferroicity by different metal halides.

4. Preparation of 2D multiferroic materials

4.1 Fabrication methods of 2D materials

The current preparation methods of 2D materials can be roughly classified into two categories: one is the top-down method, which refers to the exfoliation of bulk crystals into few-layer or monolayer 2D materials by certain technical means, mainly including mechanical exfoliation method, liquid phase ultrasonic exfoliation method, and ion intercalation assisted exfoliation method. By implying this type of method, materials with a layered structure that are combined by electrostatic interaction, a hydrogen bond or weak van der Waals force, are easily separated by external forces to obtain thin 2D nanosheets. The bottom-up method is another path to obtain 2D materials, in which small particles (such as atoms, molecules, nanoparticles, *etc.*) grow into 2D nanomaterials through the interaction between particles, typically vapour deposition.

4.1.1 Top-down methods. Within the top-down concept, 2D materials can be obtained mainly by exfoliation methods. Generally, normal force and lateral force are the two main mechanical mechanisms to exfoliate bulk or multi-layer materials into thin films. In terms of these two mechanical approaches, several mechanical exfoliation strategies are discussed.

Mechanical exfoliation method. The mechanical exfoliation method is the first technical method used to prepare 2D layered materials. A preparation process using the mechanical exfoliation method is illustrated in Fig. 6(a). In this process, the normal force exerted by the scotch tape on the surface of the multilayer material is used to overcome the van der Waals attraction between adjacent flakes. Single-layer material can be achieved by repeating this normal force numerous times. This method is the fastest and easy-to-operate approach to obtain 2D materials. Compared with other methods, the sample quality prepared by this method is high, and it is usually used for basic scientific research in the laboratory, that is, the research of physical properties and electrical devices. However, this method has poor repeatability, is time-consuming, and has low yield, making it difficult for extensive industrial applications.

Liquid phase ultrasonic exfoliation method. Due to the drawbacks of the mechanical exfoliation method that suffers from low yield, one possible solution is to exfoliate the layered compound in the liquid to produce a large number of dispersed nanosheets, which will allow obtaining a large number of 2D materials that can be processed by existing industrial technologies. In the first report of this method, graphene dispersion was obtained by dispersing graphite powder in specific organic solvents, sonication and centrifugation, which opened a whole new outlook for the low-cost and large-scale yield of graphene. One benefit of this method is that it is easy to produce graphene. The biggest disadvantage is that the graphene concentration is extremely low, which is far from practical applications. At present, the exfoliation mechanism of common strategies in the liquid phase originates from liquid cavitation, as shown in Fig. 6(b). In the sonication method, ultrasonic waves generate cavitation bubbles, which collapse into high-energy jets, destroy layered crystallites and produce exfoliated nanosheets. This technology is considered to be very successful in liquid-phase exfoliation of graphene, although it still has several shortcomings of sonication, such as basal and edges planes.

Intercalation assisted exfoliation method. Intercalation assisted exfoliation strategy, where ions or molecules can be inserted between the layers of the multilayer material to reduce the energy barrier of exfoliation, increase the layer spacing and weaken the interlayer adhesion, can achieve a large-scale and high-quality controllable synthesis of materials, which helps to exfoliate the layer with the help of gentle mechanical forces. A schematic description of the intercalation assisted exfoliation method is shown in Fig. 6(c). According to the different intercalants, this strategy can be divided into three categories: molecular intercalation, lithium intercalation and electrochemical intercalation assisted exfoliation.
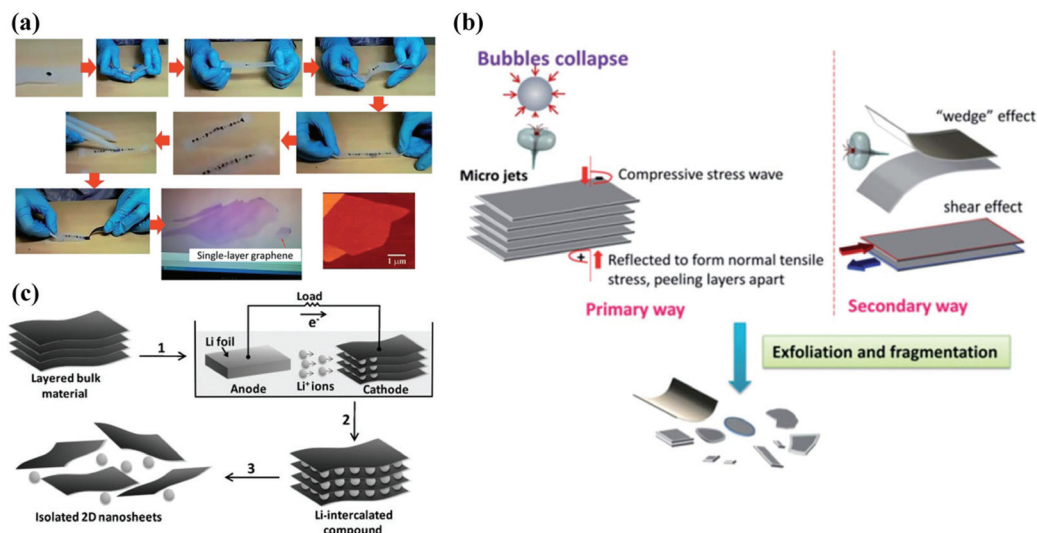
Fig. 6 Schematic diagram of top-down methods. (a) Flow chart of mechanical exfoliation method based on scotch tape. Reproduced with permission.[97] Copyright 2015, The Royal Society of Chemistry. (b) Illustration of the liquid phase ultrasonic exfoliation method. Reproduced with permission.[97] Copyright 2015, The Royal Society of Chemistry. (c) Schematic diagram of the intercalation assisted exfoliation method. Reproduced with permission.[98] Copyright 2011, Wiley-VCH.

4.1.2 Bottom-up methods. Bottom-up methods depend on the chemical reaction of molecular building blocks to form co-valently linked 2D networks, among which vapour phase deposition[99] is a typical technique that prepares atomic-scale films or thin flakes by directly depositing anticipated vapour-phase compounds on specific substrates. This technology can realize the preparation of large-area uniform, high-quality, and highly controllable 2D materials. Normally, chemical vapour deposition (CVD) and physical vapour deposition (PVD) are two main methods.

CVD is a kind of technology that uses plasma excitation, heating and other methods to chemically react reactants under certain temperature and gaseous conditions and deposit the resulting solid substances on the surface of the substrate at an appropriate position to prepare a solid thin film. Using this method can obtain 2D materials[100] with very scalable size, controllable thickness, and high quality, making it positive for the application in the electronic industry.

PVD is a thin film preparation technique in which materials are deposited on substrates by means of evaporation, emission and ion beam evaporation in a high vacuum environment. The vacuum coating equipment is a vacuum evaporation coating machine, vacuum magnetron sending coating machine and vacuum ion coating machine. This technique is one of the most efficient methods for preparing thin-film materials in industry and commerce. The reason is that the PVD method can directly prepare 2D materials on the substrate without additional chemical reactions.

4.2 Fabrication methods of 2D multiferroics

At present, the research on 2D multiferroic materials is still on the theoretical prediction, and few of them have been success-fully prepared in the experiment. There are mainly several methods for the synthesis for the existing 2D multiferroic materials: CVD, PVD, exfoliation and other strategies.

4.2.1 CVD method. In 2D multiferroic material Fe-doped $In_2Se_3(Fe_{0.16}In_{1.84}Se_3)$, In_2Se_3 single-layer[101] has been synthesized on mica substrates at 660 °C by CVD using H_2/Ar mixture as the carrier gas and powders of indium oxide (In_2O_3) and selenium (Se) as precursors (Fig. 7(a)). For the synthesis of 2D group IV monochalcogenides with ferroelectric and ferroe-lastic properties, such as SnS,[102] SnS_2 single crystal substrate in an ultrahigh vacuum is degassed at 300 °C for 3 h prior to growth and SnS was evaporated by congruent sublimation from purified SnS powder in a custom-built Knudsen cell (Fig. 7(b)). This strategy has been also successfully used to synthesize single-layer and few-layer transition metal dichalcogen-ide, including $TiSe_2$,[103] TaS_2,[104] $NbSe_2$,[105] NbS_2,[106] VX_2 (X = S, Se).[107] For example, the process of synthesizing VX_2 flakes with FE and FM by the CVD method is shown in Fig. 7(c). In this process, VCl_3 and S/Se powders are served as precursors, and hexagonal boron nitride flakes on SiO_2/Si substrates are placed at different locations downstream of the furnace, keeping the reaction temperature at about 650°.

4.2.2 PVD method. The PVD method recrystallizes the material through the gas–solid phase reaction to obtain 2D thin-film materials. Up to now, many 2D multiferroic materials have been prepared using PVD technology. In 2015, high-quality monolayered α-In_2Se_3[108] was prepared by this strategy under atmospheric pressure, and the synthesis process is shown in Fig. 7(d). Recently, Botcha et al.[109] fabricated various In_2Se_3 nanostructures on SiO_2/Si substrate using a simple and single-step PVD method, without using metal seed layer on the substrates.
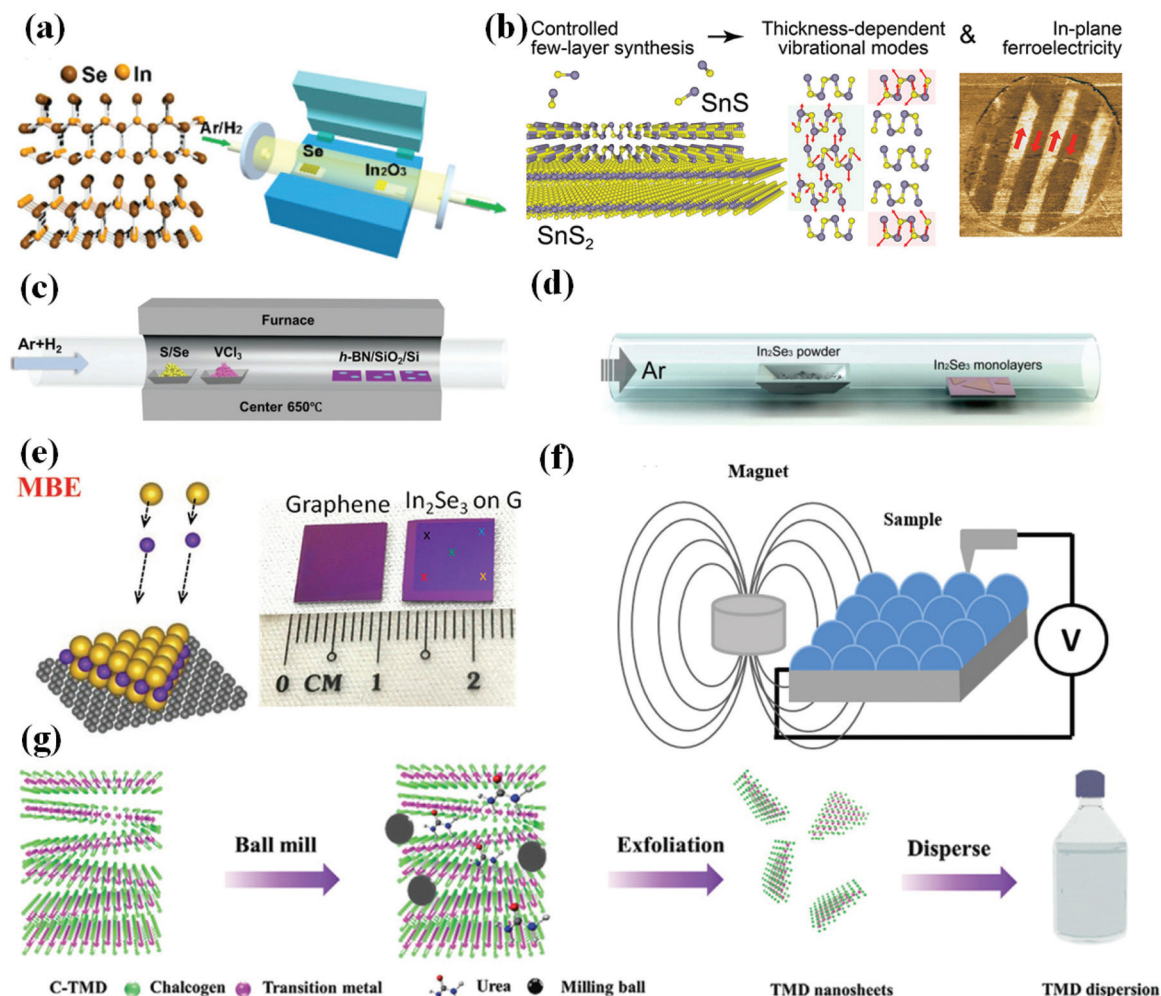
Fig. 7 Preparation methods of two-dimensional multiferroic material. (a) Schematic diagram of the growth process of 2D In_2Se_3 synthesized by the CVD method. Reproduced with permission.[101] Copyright 2016, American Chemical Society. (b) Synthesis of few-layer SnS on SnS_2 van der Waals substrates. Reproduced with permission.[102] Copyright 2021, Elsevier. (c) Illustrations of synthesis of VX_2 by CVD strategy. Reproduced with permission.[107] Copyright 2018, Wiley-VCH. (d) Process of preparing α-In_2Se_3 by PVD method. Reproduced with permission.[108] Copyright 2015, American Chemical Society. (e) Synthesis of VSe_2 monolayers by MBE technology. Reproduced with permission.[117] Copyright 2018, Wiley-VCH;[110] Copyright 2018, Springer Nature. (f) Schematic drawing of MS setup. Reproduced with permission.[118] Copyright 2020, Springer Nature. (g) Schematic illustration of the preparation of MX_2 nanosheets by using a solid phase exfoliation strategy. Reproduced with permission.[115] Copyright 2020, Wiley-VCH.

Molecular beam epitaxy growth (MBE) and magnetron sputtering (MS) in PVD are commonly used to prepare 2D multiferroic materials. In 2018, Poh *et al.*[110] used low-temperature MBE technology to synthesize high-quality and large-area monolayer α-In_2Se_3 on graphene, thereby simplifying the manufacturing of high-performance ferroelectric Schottky diodes for memory applications. The prepared α-In_2Se_3 film is shown in Fig. 7(e). In addition to the preparation of transition metal dichalcogenide films by CVD technology, experiments have proved that they can also be successfully grown by using the MBE method. Peng[111] has obtained a single-layer thickness of $TiSe_2$, demonstrating an alternative method for manufacturing single and few-layer transition metal dichalcogenide materials. In 2005, Posadas *et al.*[112] successfully synthesized epitaxial thin films of multiferroic

$YMnO_3$ on GaN/sapphire, which is helpful to study the origin of multiferroicity and the interaction between FE and magnetism in this material. Recently, iodide films (such as CrI_3)[113] have also been reported to be able to be prepared by MBE technology.

In the process of magnetron sputtering (Fig. 7(f)), a target (or cathode) plate is bombarded by energetic ions generated in a glow discharge plasma situated in front of the target, which is a classic physical deposition process whereby the bombardment process ejects atoms from the target as a result of a collision cascade that subsequently deposits the film. This strategy has been used to prepare perovskite bilayer, such as YMnO thin films,[114] and obtained Ca-based double-perovskite bilayer[72] have been confirmed to be 2D multiferroic materials with electromagnetic effect.

4.2.3 Exfoliation method. Zhang et al.[115] prepared 18 kinds of MX_2 (M = Mo, W, V, Nb, Ta, Ti, X = Te, Se, S) nanosheets by using a solid phase exfoliation strategy with high productivity, feasibility and repeatability (Fig. 7(g)). The exfoliated 2D transition metal dichalcogenides nanosheets can be easily processed as powders, water dispersions, and thin films, offering exciting opportunities for a wide range of applications from electronics to energy storage. Liu et al.[79] verified that it is feasible to exfoliate one GaTeCl monolayer from the GaTeCl bulk, and found that the GaTeCl monolayer has giant FA and large ferroelectric polarization. Similarly, other 2D multiferroic materials, including single-layer Nb_2ATe_4 (A = Si, Ge),[88] FeOOH monolayer[89] and nanosheet NiH_2SeO_4,[85] can also be obtained by mechanical peeling of single crystals (transparent glue method) owing to the weak interlayer interaction in their crystals.

4.2.4 Sol–gel method. In addition to the commonly used methods for preparing 2D multiferroic materials mentioned above, the sol–gel method is also a popular process for preparing perovskite thin films because of its advantages of low fabrication cost, relatively easy stoichiometric control and high deposition rate. In 2003, Kim et al.[116] successfully deposited $YMnO_3$ thin films on the Pt (111)/Ti/SiO$_2$/Si and Si (100) substrates by sol–gel process using alkoxides.

5. Summary and outlook

In summary, we review the research progress of 2D multiferroic materials and discuss different classifications of 2D multiferroics (Table 1 summarizes some of the reported 2D multiferroic materials). Preparation methods of these materials are also reviewed. Despite many 2D multiferroic materials having been predicted and studied, the exploration of 2D multiferroicity is still in the early stages, especially experimentally. In the process of designing and searching for 2D multiferroic materials, theoretical calculations usually provide directional suggestions for exploring and proving 2D multiferroic properties. Although it is still very challenging to observe stable multiferroicity at room temperature in existing 2D materials, we will have more and more methods to discover new 2D multiferroic materials, including potential physical properties and internal mechanism characterization and manufacturing methods. Since exploring new 2D multiferroic materials has always been an attractive topic, new basic research may address weak electromagnetic coupling effects, depolarization effects, etc. At the same time, the exploration of 2D multiferroicity will also contribute to new scientific frontiers, such as spintronics and valley electronics, which will bring exciting technological advances. Finally, with the discovery of more and more 2D multiferroic materials so far, it is expected that minimization and integration of functional electronics will soon be realized, which will usher in a new scientific era.

Since the beginning of the 21st century, the research and development of new materials have become fierce, especially the exploration of micro and nanomaterials is changing with each passing day. As a large family of new materials, 2D materials are favoured by academia because of their unique physical properties. From the birth of graphene in 2004 to the synthesis of MXene in 2011, the research and application of a new generation of 2D materials have sprung up. However, the research on 2D multiferroic materials has just begun.

The ability of multiferroics to regulate magnetism using electric fields via their magnetoelectric coupling has been the major technical push for their exploration. Because the generation of electric fields uses considerably less energy than the production of magnetic fields utilized in most present magnetism-based devices, such a capacity might be technologically revolutionary. Multiferroicity has been utilized to tackle fundamental cosmological and particle physics difficulties. The fact that any electric dipole moment with symmetry requirements takes the same axis as its magnetic dipole moment has been utilized to discover the electric dipole moment of the electron, which is ideally multiferroic. When the ferroelectric polarization is switched in the applied electric field, the developed multiferroic material (Eu, Ba)TiO$_3$ is utilized to monitor the change in the net magnetic moment, allowing the upper limit of the achievable value of the electronic electric dipole moment to be retrieved. This number is significant because it indicates the amount of time-reversal symmetry breaches in the cosmos, which places severe constraints on the theory of basic particle physics.

2D multiferroic materials have a wide range of application prospects in the following fields (Fig. 8). 1. Low energy data storage:[121] unlike traditional storage devices that use electricity to calculate and magnets to store data, memories based on 2D multiferroic materials use electricity to calculate and store data simultaneously. 2. Spintronics:[122] spintronic devices based on 2D ferromagnetic materials are promising as spintronic devices rely on nanomaterials with a size smaller than the spin relaxation length and adjustable interface characteristics. However, the disordered system obtained by the traditional method usually has low magnetic properties and is not suitable for the application. Therefore, searching for 2D materials with inherent magnetic properties is the ultimate goal of spintronics for 2D materials. 3. Nanoelectronics:[123] electronic devices based on 2D multiferroic materials can make the devices have higher rectification characteristics and easier to realize the manufacture of PN junctions, thereby providing a way for nano-devices with diverse functions. However, the preparation and growth mechanism of 2D multiferroic materials is still in the exploratory stage, which limits the development of 2D multiferroic equipment. 4. Power electronics:[81] 2D multiferroic materials with piezoelectric effect have become the main focus of energy harvesting application research, ranging from small-scale low-power electronic devices to large-scale industrial applications, such as self-

Table 1 2D multiferroic materials

	Materials	Type	Classification I/II	Intrinsic/extrinsic	Date
1	$FeTe_2O_5Br$[76]	Ferroelectric–ferromagnetic	II	Intrinsic	2013
2	C_6N_8H organic[33]	Ferroelectric–ferromagnetic	I	Intrinsic	2017
3	2D ferromagnets like MXene, VS_2, and MoN_2[11]	Ferroelectric–ferromagnetic	I	Intrinsic	2017
4	Halogen-intercalated phosphorene bilayer[93]	Ferroelectric–ferromagnetic	I	Extrinsic	2017
5	2D CrN and CrB_2 systems[82]	Ferroelectric–ferromagnetic	I	Intrinsic	2017
6	Monolayer chromium triiodide (CrI_3)[27]	Ferroelectric–ferromagnetic	I	Extrinsic	2018
7	Double transition metal carbides $Hf_2MC_2T_2$[29]	Ferroelectric–ferromagnetic	II	Intrinsic	2018
8	Transition metal phosphorus chalcogenides[28]	Ferroelectric–ferromagnetic	I	Intrinsic	2018
9	CH_2OCH_3-Functionalized germanene[95]	Ferroelectric–ferromagnetic	I	Extrinsic	2018
10	$VOCl_2$ monolayer[30]	Ferroelectric–ferromagnetic	I	Intrinsic	2018
11	Transition-metal halide monolayer $(CrBr_3)_2Li$[91]	Ferroelectric–ferromagnetic	I	Extrinsic	2018
12	$NiCl_2$-Functionalized C_2N[96]	Ferroelectric–ferromagnetic	I	Extrinsic	2019
13	Ba or Ti deficient $BaTiO_3$ ultrathin film[92]	Ferroelectric–ferromagnetic	I	Extrinsic	2019
14	Monolayer $CuCrP_2S_6$[13]	Ferroelectric–ferromagnetic	I	Intrinsic	2019
15	Fe-Doped In_2Se_3 $(Fe_{0.16}In_{1.84}Se_3)$[66]	Ferroelectric–ferromagnetic	I	Intrinsic	2019
16	Monolayer γ-GeSe[64]	Ferroelectric–ferromagnetic	I	Intrinsic	2019
17	Mn (Fe)-Doped SnTe monolayer[67]	Ferroelectric–ferromagnetic	I	Intrinsic	2019
18	$ReWCl_6$ monolayer[83]	Ferroelectric–ferromagnetic	I	Intrinsic	2020
19	2D $ScCrP_2Se_6$ monolayer[68]	Ferroelectric–ferromagnetic	I	Intrinsic	2020
20	Li-Decorated α-Fe_2O_3 ($Li@Fe_2O_3$) monolayer[94]	Ferroelectric–ferromagnetic	I	Extrinsic	2020
21	$BaTiO_3$ ultrathin film[34]	Ferroelectric–ferromagnetic	I	Intrinsic	2020
22	Double-perovskite bilayer with the Fe–Os[71]	Ferroelectric–ferromagnetic	I	Intrinsic	2020
23	2D organometallic framework[84]	Ferroelectric–ferromagnetic	I	Intrinsic	2020
24	NiH_2SeO_4 single crystals[85]	Ferroelectric–ferromagnetic	I	Intrinsic	2020
25	VOF_2 monolayer[74]	Ferroelectric–ferromagnetic	I	Intrinsic	2020
26	2D van der Waals heterostructures $CuInP_2S_6$/InSe[69]	Ferroelectric–ferromagnetic	I	Intrinsic	2020
27	2D bilayer VS_2[78]	Ferroelectric–ferromagnetic	I	Intrinsic	2020
28	CrN monolayer[86]	Ferroelectric–ferromagnetic	I	Intrinsic	2020
29	2D thin-layer $CuCrX_2$ (X = S or Se)[36]	Ferroelectric–ferromagnetic	I	Intrinsic	2020
30	VOI_2[31]	Ferroelectric–ferromagnetic	I	Intrinsic	2020
31	NiH_2SeO_4[85]	Ferroelectric–ferromagnetic	I	Intrinsic	2020
32	2D $VOCl_2$ monolayer[87]	Ferroelectric–ferromagnetic	I	Intrinsic	2021
33	2D $RMnO_3$ (R = Tb, Lu and Y)[70]	Ferroelectric–ferromagnetic	I	Intrinsic	2021
34	Perovskite bilayer: $Ca_3Mn_2O_7$ bilayer[73]	Ferroelectric–ferromagnetic	I	Intrinsic	2021
35	Ca-Based double-perovskite bilayer[72]	Ferroelectric–ferromagnetic	I	Intrinsic	2021
36	Hole-doped and arsenic-doped monolayer α-In_2Se_3[65]	Ferroelectric–ferromagnetic	I	Intrinsic	2021
37	$CrNCl_2$ monolayer[77]	Ferroelectric–ferromagnetic	I	Intrinsic	2021
38	VOF monolayer[75]	Ferroelectric–ferromagnetic	I	Intrinsic	2021
39	SnS, SnSe, GeS, and GeSe monolayers[12,39]	Ferroelectric–ferroelastic	N/A	Intrinsic	2016
40	Group IV monochalcogenides[40]	Ferroelectric–ferroelastic	N/A	Intrinsic	2017
41	Bi_2O_2Se, Bi_2O_2S and Bi_2O_2Te[41]	Ferroelectric–ferroelastic	N/A	Intrinsic	2017
42	Boron pentaphosphide (BP_5) monolayer[14]	Ferroelectric–ferroelastic	N/A	Intrinsic	2017
43	GaTeCl monolayer[79]	Ferroelectric–ferroelastic	N/A	Intrinsic	2018
44	Silver and copper monohalides[42]	Ferroelectric–ferroelastic	N/A	Intrinsic	2019
45	Nb_2SiTe_4 and Nb_2GeTe_4[88]	Ferroelectric–ferroelastic	N/A	Intrinsic	2019
46	β-GeSe and α-SnTe monolayer[119]	Ferroelectric–ferroelastic	N/A	Intrinsic	2021
47	Bilayer ZrI_2[43]	Ferroelectric–ferroelastic	N/A	Intrinsic	2021
48	α-SnO[45]	Ferromagnetic–ferroelastic	N/A	Intrinsic	2016
49	H type Janus-VSSe[81]	Ferromagnetic–ferroelastic	N/A	Intrinsic	2018
50	CrSX (X = Cl, Br, I) monolayers[35]	Ferromagnetic–ferroelastic	N/A	Intrinsic	2020
51	Monolayer α-PbO[120]	Ferromagnetic–ferroelastic	N/A	Extrinsic	2020
52	Tetragonal structures XOBr (X = Tc, Ru)[47]	Ferromagnetic–ferroelastic	N/A	Intrinsic	2020
53	Vanadium tetrafluoride (VF_4) monolayer[80]	Ferromagnetic–ferroelastic	N/A	Intrinsic	2020
54	Single-layer AgF_2[44]	Ferromagnetic–ferroelastic	N/A	Intrinsic	2020
55	Li-Doped GdI_3 monolayer[63]	Ferromagnetic–ferroelastic	N/A	Intrinsic	2021
56	Transition-metal-doped group-IVmonochalcogenides[62]	Ferroelectric–ferromagnetic–ferroelastic	N/A	Intrinsic	2018
57	FeOOH monolayer[89]	Ferroelectric–ferromagnetic-ferroelastic	N/A	Intrinsic	2020

powered sensor devices,[124] environmental monitoring, and large-scale power generation. 5. Sensor & actuator:[125] 2D multiferroic with piezoelectric effect are also ideal materials for sensors and actuators with wearable and low power consumption. 6. Microwave and Radio Frequency (RF) devices: the multiferroic heterojunction with both ferroelectric and ferromagnetic properties can achieve voltage-controlled magnetic properties through the strain-induced magnetoelectric coupling effect. Therefore, the microwave and RF device prepared by this mechanism can meet the requirements of miniaturization, ultra-fast response and low power consumption, and can realize new functionality. The development of such

Fig. 8 Prospects of 2D multiferroic materials. Illustration of the low energy data storage, Reproduced with permission,[121] Copyright 2020, Wiley-VCH. Illustration of nanoelectronics, Reproduced with permission,[123] Copyright 2019, Springer Nature. Illustration of sensors & actuators. Reproduced with permission,[125] Copyright 2020, The Royal Society of Chemistry. Illustration of power electronics, Reproduced with permission.[81] Copyright 2019, The Royal Society of Chemistry.

devices provides broad prospects for the realization of next-generation tunable magnetic microwave components, ultra-low power electronic devices and spintronic components.

Conflicts of interest

There are no conflicts to declare.

Acknowledgements

References

1 K. Zhai, D.-S. Shang, Y.-S. Chai, G. Li, J.-W. Cai, B.-G. Shen and Y. Sun, *Adv. Funct. Mater.*, 2018, **28**, 1705771.

2 M. Bichurin, R. Petrov, V. Leontiev, G. Semenov and O. Sokolov, *Sensors*, 2017, **17**, 1271.

3 Z. Yang, S. Zhou, J. Zu and D. Inman, *Joule*, 2018, **2**, 642–697.

4 N. Hiremath, R. Guntupalli, V. Vodyanoy, B. A. Chin and M.-K. Park, *Sens. Actuators, B*, 2015, **210**, 129–136.

5 J. Zhang, B. Wang, M. Tebyetekerwa, Y. Zhu, B. Liu, H. T. Nguyen, S. Tian, Y. Zhang and Y. Lu, *J. Mater. Chem. C*, 2019, **7**, 15074–15081.

6 M. Gao, P. Wang, L. Jiang, B. Wang, Y. Yao, S. Liu, D. Chu, W. Cheng and Y. Lu, *Energy Environ. Sci.*, 2021, **14**, 2114–2157.

7 Y. Zhu, Z. Li, L. Zhang, B. Wang, Z. Luo, J. Long, J. Yang, L. Fu and Y. Lu, *ACS Appl. Mater. Interfaces*, 2018, **10**, 43291–43298.

8 Z. Lu, G. P. Neupane, G. Jia, H. Zhao, D. Qi, Y. Du, Y. Lu and Z. Yin, *Adv. Funct. Mater.*, 2020, **30**, 2001127.

9 J. Pei, J. Yang, T. Yildirim, H. Zhang and Y. Lu, *Adv. Mater.*, 2019, **31**, e1706945.

10 K. S. Novoselov, A. K. Geim, S. V. Morozov, D. Jiang, Y. Zhang, S. V. Dubonos, I. V. Grigorieva and A. A. Firsov, *Science*, 2004, **306**, 666–669.

11 L. Li and M. Wu, *ACS Nano*, 2017, **11**, 6382–6388.

12 M. Wu and X. C. Zeng, *Nano Lett.*, 2016, **16**, 3236–3241.

13 Y. Lai, Z. Song, Y. Wan, M. Xue, C. Wang, Y. Ye, L. Dai, Z. Zhang, W. Yang, H. Du and J. Yang, *Nanoscale*, 2019, **11**, 5163–5170.

14 H. Wang, X. Li, J. Sun, Z. Liu and J. Yang, *2D Mater.*, 2017, **4**, 045020.

15 K. Cho, J. Yang and Y. Lu, *J. Mater. Res.*, 2017, **32**, 2839–2847.

16 E. Blundo, C. Di Giorgio, G. Pettinari, T. Yildirim, M. Felici, Y. Lu, F. Bobba and A. Polimeni, *Adv. Mater. Interfaces*, 2020, **7**, 2000621.

17 C. Di Giorgio, E. Blundo, G. Pettinari, M. Felici, Y. Lu, A. M. Cucolo, A. Polimeni and F. Bobba, *Adv. Mater. Interfaces*, 2020, **7**, 2001024.

18 D. Tedeschi, E. Blundo, M. Felici, G. Pettinari, B. Liu, T. Yildrim, E. Petroni, C. Zhang, Y. Zhu, S. Sennato, Y. Lu and A. Polimeni, *Adv. Mater.*, 2019, **31**, e1903795.

19 A. R. Khan, T. Lu, W. Ma, Y. Lu and Y. Liu, *Adv. Electron. Mater.*, 2020, **6**, 1901381.

20 S. Rahman, B. Liu, B. Wang, Y. Tang and Y. Lu, *ACS Appl. Mater. Interfaces*, 2021, **13**, 7423–7433.

21 B. Wen, Y. Zhu, D. Yudistira, A. Boes, L. Zhang, T. Yidirim, B. Liu, H. Yan, X. Sun, Y. Zhou, Y. Xue, Y. Zhang, A. Mitchell, H. Zhang and Y. Lu, *ACS Nano*, 2019, **13**, 5335–5343.

22 L. Zhang, H. Yan, X. Sun, M. Dong, T. Yildirim, B. Wang, B. Wen, G. P. Neupane, A. Sharma, Y. Zhu, J. Zhang, K. Liang, B. Liu, H. T. Nguyen, D. Macdonald and Y. Lu, *Nanoscale*, 2019, **11**, 418–425.

23 M. Tebyetekerwa, J. Zhang, K. Liang, T. Duong, G. P. Neupane, L. Zhang, B. Liu, T. N. Truong, R. Basnet, X. Qiao, Z. Yin, Y. Lu, D. Macdonald and H. T. Nguyen, *Adv. Mater.*, 2019, **31**, e1900522.

24 M. An and S. Dong, *APL Mater.*, 2020, **8**, 110704.

25 L. W. Martin, S. P. Crane, Y. H. Chu, M. B. Holcomb, M. Gajek, M. Huijben, C. H. Yang, N. Balke and R. Ramesh, *J. Phys.: Condens. Matter*, 2008, **20**, 434220.

26 E. Ascher, H. Rieder, H. Schmid and H. Stössel, *J. Appl. Phys.*, 1966, **37**, 1404–1405.

27 Y. Zhao, L. Lin, Q. Zhou, Y. Li, S. Yuan, Q. Chen, S. Dong and J. Wang, *Nano Lett.*, 2018, **18**, 2943–2949.

28 W. Wan, C. Liu, W. Xiao and Y. Yao, *Appl. Phys. Lett.*, 2017, **111**, 132904.

29 J. J. Zhang, L. Lin, Y. Zhang, M. Wu, B. I. Yakobson and S. Dong, *J. Am. Chem. Soc.*, 2018, **140**, 9768–9773.

30 H. Ai, X. Song, S. Qi, W. Li and M. Zhao, *Nanoscale*, 2019, **11**, 1103–1110.

31 N. Ding, J. Chen, S. Dong and A. Stroppa, *Phys. Rev. B*, 2020, **102**, 165129.

32 C. Xu, P. Chen, H. Tan, Y. Yang, H. Xiang and L. Bellaiche, *Phys. Rev. Lett.*, 2020, **125**, 037203.

33 Z. Tu, M. Wu and X. C. Zeng, *J. Phys. Chem. Lett.*, 2017, **8**, 1973–1978.

34 H. Gao, T. Lin, Y. Yan, K. Fu, Y. Liu and X. Liu, *Phys. Chem. Chem. Phys.*, 2020, **22**, 18284–18293.

35 J. Qi, H. Wang, X. Chen and X. Qian, *Appl. Phys. Lett.*, 2018, **113**, 043102.

36 T. Zhong, X. Li, M. Wu and J.-M. Liu, *Natl. Sci. Rev.*, 2020, **7**, 373–380.

37 A. R. Khan, B. Liu, L. Zhang, Y. Zhu, X. He, L. Zhang, T. Lü and Y. Lu, *Adv. Opt. Mater.*, 2020, **8**, 2000441.

38 A. R. Khan, B. Liu, T. Lü, L. Zhang, A. Sharma, Y. Zhu, W. Ma and Y. Lu, *ACS Nano*, 2020, **14**, 15806–15815.

39 H. Wang and X. Qian, *2D Mater.*, 2017, **4**, 015042.

40 H. Wang and X. Qian, *Nano Lett.*, 2017, **17**, 5027–5034.

41 M. Wu and X. C. Zeng, *Nano Lett.*, 2017, **17**, 6309–6314.

42 Y. Gao, M. Wu and X. C. Zeng, *Nanoscale Horiz.*, 2019, **4**, 1106–1112.

43 T. Zhang, Y. Liang, X. Xu, B. Huang, Y. Dai and Y. Ma, *Phys. Rev. B*, 2021, **103**, 165420.

44 X. Xu, Y. Ma, T. Zhang, C. Lei, B. Huang and Y. Dai, *Nanoscale Horiz.*, 2020, **5**, 1386–1393.

45 L. Seixas, A. S. Rodin, A. Carvalho and A. H. Castro Neto, *Phys. Rev. Lett.*, 2016, **116**, 206803.

46 B. Xu, S. Li, K. Jiang, J. Yin, Z. Liu, Y. Cheng and W. Zhong, *Appl. Phys. Lett.*, 2020, **116**, 052403.

47 Z.-x. Pang, W.-x. Ji, C.-w. Zhang, P.-j. Wang and P. Li, *Chem. Phys. Lett.*, 2021, **763**, 138163.

48 D. Khomskii, *Physics*, 2009, **2**, DOI: 10.1103/Physics.2.20.

49 S. Dong, J.-M. Liu, S.-W. Cheong and Z. Ren, *Adv. Phys.*, 2015, **64**, 519–626.

50 Y. Bai, H. Zhao, J. Chen, Y. Sun and S. Zhao, *Ceram. Int.*, 2016, **42**, 10304–10309.

51 P. R. Mickel, H. Jeen, P. Kumar, A. Biswas and A. F. Hebard, *Phys. Rev. B*, 2016, **93**, 134205.

52 L. H. d. S. Lacerda and S. R. de Lazaro, *J. Magn. Magn. Mater.*, 2020, **500**, 166364.

53 F. Y. Nad, P. Monceau, C. Carcel and J. M. Fabre, *Synth. Met.*, 2003, **133–134**, 265–267.

54 N. Ikeda, H. Ohsumi, K. Ohwada, K. Ishii, T. Inami, K. Kakurai, Y. Murakami, K. Yoshii, S. Mori, Y. Horibe and H. Kito, *Nature*, 2005, **436**, 1136–1138.

55 P. Jarillo-Herrero, S. Sapmaz, C. Dekker, L. P. Kouwenhoven and H. S. Van Der Zant, *Nature*, 2004, **429**, 389–392.

56 Y. J. Choi, H. T. Yi, S. Lee, Q. Huang, V. Kiryukhin and S. W. Cheong, *Phys. Rev. Lett.*, 2008, **100**, 047601.

57 B. B. Van Aken, T. T. Palstra, A. Filippetti and N. A. Spaldin, *Nat. Mater.*, 2004, **3**, 164–170.

58 N. M. Avram, M. G. Brik and E. L. Andreici, *Phys. Scr.*, 2014, **T162**, 014020.

59 M. Fiebig, T. Lottermoser, D. Meier and M. Trassin, *Nat. Rev. Mater.*, 2016, **1**, 16046.

60 S. M. Yakout, *J. Supercond. Novel Magn.*, 2021, **34**, 317–338.

61 Y. Tokura, S. Seki and N. Nagaosa, *Rep. Prog. Phys.*, 2014, **77**, 076501.

62 L. Yang, M. Wu and K. Yao, *Nanotechnology*, 2018, **29**, 215703.

63 H. You, Y. Zhang, J. Chen, N. Ding, M. An, L. Miao and S. Dong, *Phys. Rev. B*, 2021, **103**, L161408.

64 C. Liu, S. Guan, H. Yin, W. Wan, Y. Wang and Y. Zhang, *Appl. Phys. Lett.*, 2019, **115**, 252904.

65 X. Duan, J. Huang, B. Xu and S. Liu, *Mater. Horiz.*, 2021, **8**, 2316–2324.

66 H. Yang, L. Pan, M. Xiao, J. Fang, Y. Cui and Z. Wei, *Sci. China Mater.*, 2020, **63**, 421–428.

67 Y. Liu, W. Zhou, G. Tang, C. Yang, X. Wang and J. Hong, *J. Phys. Chem. C*, 2019, **123**, 28919–28924.

68 X. Feng, J. Liu, X. Ma and M. Zhao, *Phys. Chem. Chem. Phys.*, 2020, **22**, 7489–7496.

69 Z. Zhu, X. Chen, W. Li and J. Qi, *J. Mater. Chem. C*, 2020, **8**, 17342–17348.

70 G. E. Tongue Magne, R. M. Keumo Tsiaze, A. J. Fotué, N. M. Hounkonnou and L. C. Fai, *Phys. Lett. A*, 2021, **400**, 127305.

71 J. Zhang, X. Shen, Y. Wang, C. Ji, Y. Zhou, J. Wang, F. Huang and X. Lu, *Phys. Rev. Lett.*, 2020, **125**, 017601.

72 X. Shen, Q. Luo, Z. Wu, Y. Zhou, J. Wang, J. Zhang, J. Su and X. Lu, *Phys. Rev. B*, 2021, **103**, L220406.

73 Y. Zhou, Z. Chen, Z. Wu, X. Shen, J. Wang, J. Zhang and H. Sun, *Phys. Rev. B*, 2021, **103**, 224409.

74 H. P. You, N. Ding, J. Chen and S. Dong, *Phys. Chem. Chem. Phys.*, 2020, **22**, 24109–24115.

75 S. Xu, F. Jia, G. Zhao, W. Wu and W. Ren, *J. Mater. Chem. C*, 2021, **9**, 9130–9136.

76 J. Chakraborty, N. Ganguli, T. Saha-Dasgupta and I. Dasgupta, *Phys. Rev. B: Condens. Matter Mater. Phys.*, 2013, **88**, 094409.

77 W. Shen, Y. Pan, S. Shen, H. Li, S. Nie and J. Mei, *Chin. Phys. B*, 2021, DOI: 10.1088/1674-1056/ac0787.

78 X. Liu, A. P. Pyatakov and W. Ren, *Phys. Rev. Lett.*, 2020, **125**, 247601.

79 S. H. Zhang and B. G. Liu, *Nanoscale*, 2018, **10**, 5990–5996.

80 L. Zhang, C. Tang and A. Du, *J. Mater. Chem. C*, 2021, **9**, 95–100.

81 J. Yang, A. Wang, S. Zhang, J. Liu, Z. Zhong and L. Chen, *Phys. Chem. Chem. Phys.*, 2018, **21**, 132–136.

82 W. Luo, K. Xu and H. Xiang, *Phys. Rev. B*, 2017, **96**, 235415.

83 M. Xu, C. Huang, Y. Li, S. Liu, X. Zhong, P. Jena, E. Kan and Y. Wang, *Phys. Rev. Lett.*, 2020, **124**, 067602.

84 X. Li, X. Li and J. Yang, *J. Phys. Chem. Lett.*, 2020, **11**, 4193–4197.

85 B. Yu, Y. Shen, S. Yang, D. Xu, J. Lin, L. Sun, B. Tian, Q. Zhu, C. Duan and Q. Zhao, *J. Mater. Chem. C*, 2020, **8**, 14812–14818.

86 J. Liang, Q. Cui and H. Yang, *Phys. Rev. B*, 2020, **102**, 220409(R).

87 A. Mahajan and S. Bhowmick, *Phys. Rev. B*, 2021, **103**, 075436.

88 T. Zhang, Y. Ma, X. Xu, C. Lei, B. Huang and Y. Dai, *J. Phys. Chem. Lett.*, 2020, **11**, 497–503.

89 X. Feng, X. Ma, L. Sun, J. Liu and M. Zhao, *J. Mater. Chem. C*, 2020, **8**, 13982–13989.

90 Y. Zhou, D. Wu, Y. Zhu, Y. Cho, Q. He, X. Yang, K. Herrera, Z. Chu, Y. Han, M. C. Downer, H. Peng and K. Lai, *Nano Lett.*, 2017, **17**, 5508–5513.

91 C. Huang, Y. Du, H. Wu, H. Xiang, K. Deng and E. Kan, *Phys. Rev. Lett.*, 2018, **120**, 147601.

92 H. Gao, Z. Yue, Y. Liu, J. Hu and X. Li, *Nanomaterials*, 2019, **9**, 269.

93 Q. Yang, W. Xiong, L. Zhu, G. Gao and M. Wu, *J. Am. Chem. Soc.*, 2017, **139**, 11506–11512.

94 J. Shang, C. Li, X. Tang, A. Du, T. Liao, Y. Gu, Y. Ma, L. Kou and C. Chen, *Nanoscale*, 2020, **12**, 14847–14852.

95 L. Kou, Y. Ma, T. Liao, A. Du and C. Chen, *Phys. Rev. Appl.*, 2018, **10**, 024043.

96 L. Li, M. Wu and X. C. Zeng, *Adv. Funct. Mater.*, 2019, **29**, 1905752.

97 M. Yi and Z. Shen, *J. Mater. Chem. A*, 2015, **3**, 11700–11715.

98 Z. Zeng, Z. Yin, X. Huang, H. Li, Q. He, G. Lu, F. Boey and H. Zhang, *Angew. Chem., Int. Ed.*, 2011, **50**, 11093–11097.

99 L. Zhang, M. Mehedi Hasan, Y. Tang, A. Raza Khan, H. Yan, T. Yildirim, X. Sun, J. Zhang, J. Zhu, Y. Zhang and Y. Lu, *Mater. Today*, 2021, DOI: 10.1016/j.mattod.2021.02.021.

100 J. Zhang, Y. Zhu, M. Tebyetekerwa, D. Li, D. Liu, W. Lei, L. Wang, Y. Zhang and Y. Lu, *ACS Appl. Nano Mater.*, 2020, **4**, 769–777.

101 W. Feng, W. Zheng, F. Gao, X. Chen, G. Liu, T. Hasan, W. Cao and P. Hu, *Chem. Mater.*, 2016, **28**, 4278–4283.

102 P. Sutter, H. P. Komsa, H. Lu, A. Gruverman and E. Sutter, *Nano Today*, 2021, **37**, 101082.

103 H. Wang, Y. Chen, M. Duchamp, Q. Zeng, X. Wang, S. H. Tsang, H. Li, L. Jing, T. Yu, E. H. T. Teo and Z. Liu, *Adv. Mater.*, 2018, **30**, 1704382.

104 W. Fu, Y. Chen, J. Lin, X. Wang, Q. Zeng, J. Zhou, L. Zheng, H. Wang, Y. He, H. He, Q. Fu, K. Suenaga, T. Yu and Z. Liu, *Chem. Mater.*, 2016, **28**, 7613–7618.

105 H. Wang, X. Huang, J. Lin, J. Cui, Y. Chen, C. Zhu, F. Liu, Q. Zeng, J. Zhou, P. Yu, X. Wang, H. He, S. H. Tsang, W. Gao, K. Suenaga, F. Ma, C. Yang, L. Lu, T. Yu, E. H. T. Teo, G. Liu and Z. Liu, *Nat. Commun.*, 2017, **8**, 394.

106 X. Wang, J. Lin, Y. Zhu, C. Luo, K. Suenaga, C. Cai and L. Xie, *Nanoscale*, 2017, **9**, 16607–16611.

107 M. Hossain, J. Wu, W. Wen, H. Liu, X. Wang and L. Xie, *Adv. Mater. Interfaces*, 2018, **5**, 800528.

108 J. Zhou, Q. Zeng, D. Lv, L. Sun, L. Niu, W. Fu, F. Liu, Z. Shen, C. Jin and Z. Liu, *Nano Lett.*, 2015, **15**, 6400–6405.

109 V. D. Botcha, Y. Hong, Z. Huang, Z. Li, Q. Liu, J. Wu, Y. Lu and X. Liu, *J. Alloys Compd.*, 2019, **773**, 698–705.

110 S. M. Poh, S. J. R. Tan, H. Wang, P. Song, I. H. Abidi, X. Zhao, J. Dan, J. Chen, Z. Luo, S. J. Pennycook, A. H. Castro Neto and K. P. Loh, *Nano Lett.*, 2018, **18**, 6340–6346.

111 J.-P. Peng, J.-Q. Guan, H.-M. Zhang, C.-L. Song, L. Wang, K. He, Q.-K. Xue and X.-C. Ma, *Phys. Rev. B: Condens. Matter Mater. Phys.*, 2015, **91**, 21113.

112 A. Posadas, J. B. Yau, C. H. Ahn, J. Han, S. Gariglio, K. Johnston, K. M. Rabe and J. B. Neaton, *Appl. Phys. Lett.*, 2005, **87**, 171915.

113 X. Cai, Z. Xu, S.-H. Ji, N. Li and X. Chen, *Chin. Phys. B*, 2021, **30**, 028102.

114 D. C. Yoo, J. Y. Lee, I. S. Kim and Y. T. Kim, *Thin Solid Films*, 2002, **416**, 62–65.

115 L. Zhang, C. Chen, J. Zhou, G. Yang, J. Wang, D. Liu, Z. Chen and W. Lei, *Adv. Funct. Mater.*, 2020, **30**, 2004139.

116 K.-T. Kim and C.-I. Kim, *J. Eur. Ceram. Soc.*, 2004, **24**, 2613–2617.

117 X. Wang, Z. Song, W. Wen, H. Liu, J. Wu, C. Dang, M. Hossain, M. A. Iqbal and L. Xie, *Adv. Mater.*, 2019, **31**, e1804682.

118 S. Meenachisundaram, N. Wakiya, C. Muthamizhchelvan, P. Gangopadhyay, N. Sakamoto and S. Ponnusamy, *J. Electron. Mater.*, 2021, **50**, 1699–1706.

119 J. Zhou and S. Zhang, *npj 2D Mater. Appl.*, 2021, **5**, 16.

120 M.-H. Zhang, X.-L. Chen, W.-X. Ji, P.-J. Wang, Y. Min and C.-W. Zhang, *Appl. Phys. Lett.*, 2020, **116**, 172105.

121 S. R. Burns, O. Paull, J. Juraszek, V. Nagarajan and D. Sando, *Adv. Mater.*, 2020, **32**, 2003711.

122 A. Hirohata and K. Takanashi, *J. Phys. D: Appl. Phys.*, 2014, **47**, 193001.

123 N. A. Spaldin and R. Ramesh, *Nat. Mater.*, 2019, **18**, 203–212.

124 Y. Sun, P. Wang, J. Lu, J. Xu, P. Wang, S. Xie, Y. Li, J. Dai, B. Wang and M. Gao, *Appl. Energy*, 2021, **286**, 116512.

125 A. Hirohata, K. Yamada, Y. Nakatani, I.-L. Prejbeanu, B. Diény, P. Pirro and B. Hillebrands, *J. Magn. Magn. Mater.*, 2020, **509**, 166711.